Electronic Supplementary Material (ESI) for Soft Matter.
This journal is © The Royal Society of Chemistry 2019

Supporting information

Ion-selective binding as a new trigger for micellization of block copolyelectrolytes with two anionic blocks

Nico Carl,*[,†,‡] Sylvain Prévost,[†] Ralf Schweins,[†] and Klaus Huber[‡]

†*Large Scale Structures Group, DS, Institut Laue-Langevin, 71 Avenue des Martyrs, CS 20 156, 38042 Grenoble, France*

‡*Physikalische Chemie, Universität Paderborn, Warburger Str. 100, 33098 Paderborn, Germany*

E-mail: carlno@ill.fr

Contents

1 Experimental details

1.1 Materials

Light water (H_2O) was purified using a Milli-Q-system (Millipore), resistivity 18.2 MΩ cm). Heavy water (D_2O, Euriso-top, France, 99.90 atom% deuterium) was filtered with 100 nm PVDF filter (Merck Millex MPSLVV033RS) prior to use. Sodium styrene sulfonate (Sigma Aldrich, France), 4,4-azobis(4-cyanovaleric acid) (Sigma Aldrich, France, >98%), 2-(2-carboxyethylsulfanylthiocarbonylsulfanyl)propionic acid (Sigma Aldrich, France), $CaCl_2 \cdot 2\,H_2O$ (Sigma Aldrich, France, >99.9%), NaCl (Sigma Aldrich, France, >99.9%), NaOH (Sigma Aldrich, France), HCl (Sigma Aldrich, France, 37%), acrylic acid (Sigma Aldrich, France, >99%), 3-(trimethylsilyl)propionic-2,2,3,3-d_4 acid sodium salt (abcr GmbH, Germany, 98 atom% deuterium), disodium ethylenediaminetetraacetic acid (Sigma Aldrich, France, >98.5%) and d_4-acrylic acid (Polymersource, Canada, >98 atom% deuterium) were used as received.

1.2 Polymer synthesis

The synthesis of $h_3-PA_{1190}PSS_{70}$ (sodium salt, the subscript numbers denote the degree of polymerization for PAA and PSS and the number of hydrogendated/deuterated protons in the PA block) will be described exemplarily.[1–3] For the blocks denoted as d_3-PA, acrylic acid was replaced by d_4 acrylic acid.

First a PSS macro RAFT agent was synthesized by dissolving 15 g of sodium styrene sulfonate (72.9 mmol), 264.5 mg of 4,4-azobis(4-cyanovaleric acid) (1.04 mmol) and 29.2 mg of 2-(2-carboxyethylsulfanylthiocarbonylsulfanyl)propionic acid (0.10 mmol) in 150 mL of deionized water at room temperature. Subsequently, the mixture was degassed by flushing with argon for 30 min. The polymerization was carried out for 15 h at 70 °C under argon atmosphere. After the reaction the product was allowed to cool down and transferred into dialysis tubing (regenerated cellulose, Spectra/Por 6 MWCO = 1 kDa). The polymer was dialyzed against a large excess of water for 3 days with exchange of water every 12 h and finally freeze

dried. Yield: 13.1 g (86 %)

In order to obtain a PA-*b*-PSS block copolymer, 1.714 g of the previously synthesized PSS macro RAFT agent (0.19 mmol), 5 mg of 4,4-azobis(4-cyanovaleric acid) (0.018 mmol) and 11.43 mL of acrylic acid (166.6 mmol) were dissolved in 69 mL of deionized water at room temperature. The mixture was flushed with argon for 30 min. The mixture was polymerized at 70 °C for 8 h. The product was allowed to cool down, brought to pH 10 by addition of 1 M NaOH and transferred into dialysis tubing (regenerated cellulose, Spectra/Por 6 MWCO = 1 kDa). The product was dialyzed against a large excess of water for 3 days with exchange of water every 12 h and finally freeze dried. Yield: 15.5 g (82 %).

Monomer conversion and block copolymer composition were determined by NMR spectroscopy. ^{1}H (^{2}H) NMR measurements were performed in D_2O (H_2O) using a Bruker Ascent 700 or Bruker AV 500. For block copolymers containing deuterated poly acrylic acid, 3-(trimethylsilyl)-1-propanesulfonic acid-d_6 sodium salt was added as a quantitative reference to be able to integrate between ^{1}H and ^{2}H spectra for the determination of the block copolymer composition. NMR spectra are shown in **Figures S2–S10**.

1.3 Sample preparation

For the sample preparation, we followed an approached used in previous works.[4–8] The total number of positive charges for all samples was adjusted to 100 mmol L^{-1}. The total concentration of positive charges [+] is

$$[+] = [\mathrm{NaCl}] + 2 \cdot [\mathrm{CaCl_2}] = 100\,\mathrm{mmol\,L^{-1}} \tag{S1}$$

with [NaCl] being the concentration of sodium chloride and [$CaCl_2$] the concentration of calcium chloride. This means a sample containing 25 mmol L^{-1} $CaCl_2$ also contained 50 mmol L^{-1} NaCl, whereas a sample containing 50 mmol L^{-1} $CaCl_2$ contains no additional NaCl. Since the final $CaCl_2$ concentration differs for the investigated samples we describe

the sample preparation for d_3−$PA_{1190}PSS_{70}$ / h_3−$PA_{1190}PSS_{70}$ and d_3−$PA_{360}PSS_{400}$ separately.

The sample preparation for d_3−$PA_{1190}PSS_{70}$ and h_3−$PA_{1190}PSS_{70}$ was identical. First, two stock solutions of the freeze-dried polymer d_3−$PA_{1190}PSS_{70}$ (or h_3−$PA_{1190}PSS_{70}$) in 100 mmol L^{-1} NaCl solution in pure H_2O or 100 mmol L^{-1} NaCl in pure D_2O were prepared at twice (8 g L^{-1}) the final concentration and adjusted to pH/pD of 9 with a 100 mmol L^{-1} NaOH solution. Mixing these two solutions in appropriate ratios resulted in a new stock solution of polymer with the selected D_2O/H_2O content. Accordingly, stock solutions of 50 mmol L^{-1} $CaCl_2$ in pure H_2O or pure D_2O were prepared by dissolving $CaCl_2 \cdot 2H_2O$ in H_2O and D_2O. As done with the polymer solutions, mixing those $CaCl_2$ solutions in adequate ratio resulted in the $CaCl_2$ solution with the selected D_2O/H_2O ratio.

Mixing of the polymer solution with the $CaCl_2$ solution of a desired contrast in a 1:1 ratio was performed under vigorous stirring and dropwise addition of $CaCl_2$ solution to the polymer solution. This resulted in a polymer concentration of 4 g L^{-1}, a $CaCl_2$ concentration of 25 mmol L^{-1} and a NaCl concentration of 50 mmol L^{-1}.

For d_3−$PA_{360}PSS_{400}$, two stock solutions (8 g L^{-1}) of the freeze-dried polymer were prepared in pure H_2O and pure D_2O and adjusted to a pH/pD of 9 with a 100 mmol L^{-1} NaOH solution. Mixing these two solutions in appropriate ratios resulted in a new stock solution of polymer with the selected D_2O/H_2O content. Analogously, stock solutions of 100 mmol L^{-1} $CaCl_2$ in pure H_2O or pure D_2O were prepared by dissolving $CaCl_2 \cdot 2H_2O$ in H_2O and D_2O. As done with the polymer solutions, mixing those $CaCl_2$ solutions in adequate ratio resulted in the $CaCl_2$ solution with the selected D_2O/H_2O ratio.

Mixing of the polymer solution with the $CaCl_2$ solution of a desired contrast in a 1:1 ratio was performed under vigorous stirring and dropwise addition of $CaCl_2$ solution to the polymer solution. This resulted in a polymer concentration of 4 g L^{-1} and a $CaCl_2$ concentration of 50 mmol L^{-1}.

The resulting solutions were allowed to equilibrate for at least 2 days prior to mea-

surement. The polymer-free solutions which served as solvent background for SANS and SAXS were prepared in a similar way by mixing a $CaCl_2$ solution with the corresponding solvent without polymer (pure water for $d_3-PA_{360}PSS_{400}$ and 100 mmol L^{-1} NaCl for $d_3-PA_{1190}PSS_{70}$/ $h_3-PA_{1190}PSS_{70}$). The usage of $CaCl_2 \cdot 2H_2O$ results in less than 0.2 vol % additional H_2O content and therefore does not influence the D_2O content.

1.4 SAXS

Small-angle X-Ray scattering was performed at the ID02 beamline of the European Synchrotron Radiation Facility (ESRF). Two sample to detector distances (10 m and 1 m) were measured at a X-Ray energy of 12.46 keV (0.0995 nm) using a Rayonix MX-170HS CCD detector to cover a q-range of $8 \cdot 10^{-3} - 6\,nm^{-1}$. Samples were filled in 2 mm quartz glass capillaries (WJM Glas Müller, Berlin, Germany). The detector images were corrected for dark and flat-field, azimuthally averaged, corrected to transmission of the direct beam and scaled to absolute intensity using water as a secondary standard.[9,10] The scattering from the solvent was subtracted from the scattering curves. Details can be found in Ref. 10. Error bars were estimated as standard deviations from measurements of at least five different positions within the capillary.

1.5 SANS

SANS measurements were performed at the D11 small angle neutron scattering instrument of the Institut Laue-Langevin (Grenoble, France). Three sample to detector distances (39.0 m collimation 40.5 m, 8.0 m collimation 8.0 m, 1.4 m collimation 5.5 m) and a neutron wavelength of 0.5 nm (FWHM 9 %) were used to cover a q-range of $2 \cdot 10^{-2} - 5\,nm^{-1}$. We used a circular neutron beam with a diameter of 15 mm. Scattered neutrons were detected with a ^{3}He MWPC detector (CERCA) with 256 × 256 pixels of 3.75 mm × 3.75 mm pixel size. Samples were filled in 2 mm Hellma 404 Quartz Suprasil cells. The sample temperature was adjusted to 25 °C using a circulating water bath. The detector images were azimuthally

averaged, corrected to transmission of the direct beam and scaled to absolute intensity using a 1 mm H_2O cell as secondary calibration standard ($\frac{d\Sigma}{d\Omega} = 0.929\,\mathrm{cm}^{-1}$) using the LAMP software. The scattering from the solvent and the incoherent background were subtracted from the scattering curves. Details for the data reduction can be found in Chapter 2 of Ref. 11.

2 Polymer characterization

2.1 NMR

We used NMR to characterize the (block) polymers as well as the macro RAFT agents and to estimate the block length and ratios. Directly at the end of the polymerization we withdrew an aliquot to determine the turnover of the reaction. In general, barely any monomer signal was visible, from which we concluded, that the monomer conversion is at least $> 95\,\%$.

In order to estimate the degree of polymerisation of the PSS macro RAFT agent we compared the signal of the RAFT polymer to the signal arising from the RAFT end group. This was possible for PSS_{70} (c.f. Figure S1), whereas for PSS_{400} we calculated M_n from the ratio RAFT agent to monomer and assuming 100 % conversion. Consequently, we determined the block ratios from the NMR spectra of the block copolymers. Based on this and the previsouly calculated length of the PSS block we determined the length of the PA block. For the polymers where we used deuterated acrylic acid, we added 3-(Trimethylsilyl)propionic-2,2,3,3-d_4 acid sodium salt (TSP$-d_4$) to be able to integrate between ^{1}H and ^{2}H spectra. The corresponding samples were measured in D_2O for the ^{1}H experiment, freeze-dried and redissolved in H_2O for the ^{2}H experiment in order to keep the amount of TSP$-d_4$ constant.

For the $h_3-PA_{100}PSS_{750}$ block copolymer we first synthesized a PA macro RAFT agent and consequently polymerized the PSS block. The estimation of the block ratios was done similar as for $PA_{1190}PSS_{70}$.

PSS_{70}: ^{1}H NMR (D_2O, 500 MHz): δ(ppm) = 0.84–1.06 (br, 3H, **d**), 1.09–2.54 (br, 3H,

c), 2.54–2.91 (br, 2H, **f**), 3.26–3.80 (br, 2H, **e**), 6.12–7.29 (br, 2H, **b**), 7.32–8.03 (br, 2H, **a**).

h_3−$PA_{1190}PSS_{70}$: ^{1}H NMR (D_2O, 500 MHz): δ(ppm) = 0.71–2.54 (br, 6H, **c**), 6.15–7.19 (br, 2H, **b**), 7.27–7.95 (br, 2H, **a**).

d_3−$PA_{1190}PSS_{70}$: ^{1}H NMR (D_2O, 700 MHz): δ(ppm) = −0.11–0.09 (s, 9H, **d**), 1.09–1.97 (br, 3H, c), 6.31–7.09 (br, 2H, b), 7.22–7.86 (br, 2H, a). ^{2}H NMR (H_2O, 107 MHz): δ(ppm) = 0.41–0.67 (br, 2D, **c**), 0.73–3.57 (br, 5D, a & **b**, 1.85–2.06 (br, 2D, **b**).

PSS_{400}: ^{1}H NMR (D_2O, 700 MHz): δ(ppm) = 0.71–2.39 (br, 3H, **c**), 6.05–7.08 (br, 2H, **a**), 7.24–7.97 (br, 2H, **a**).

d_3−$PA_{360}PSS_{400}$: ^{1}H NMR (D_2O, 700 MHz): δ(ppm) = −0.12–0.10 (s, 9H, **d**), 0.99–2.44 (br, 3H, **c**), 5.82–7.24 (br, 2H, **b**), 7.24–7.92 (br, 2H, **a**). ^{2}H NMR (H_2O, 107 MHz): δ(ppm) = 0.43–0.80 (br, 2D, **c**), 0.95–3.47 (br, 5D, **a** & **b**), 1.80–2.15 (br, 2D, **b**).

h_3−PA_{100}: ^{1}H NMR (D_2O, 500 MHz): δ(ppm) = 0.94–1.08 (s, 3H, **d**), 1.27–2.54 (br, 3H, **c**), 2.54–2.68 (br, **?** not assigned), 2.68–2.83 (br, 2H, **b**), 3.44–3.58 (br, 2H, **a**), 4.10–4.30 (br, **?** not assigned).

h_3−$PA_{100}PSS_{750}$: ^{1}H NMR (D_2O, 500 MHz): δ(ppm) = 0.98–2.34 (br, 6H, **c**), 5.83–6.89 (br, 2H, **b**), 7.13–7.74 (br, 2H, **a**).

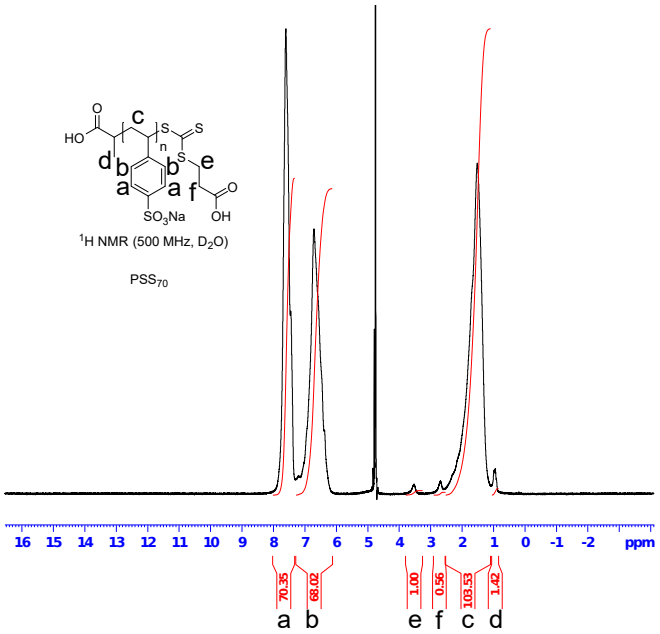

Figure S1: ^{1}H NMR spectrum of PSS_{70} in D_2O.

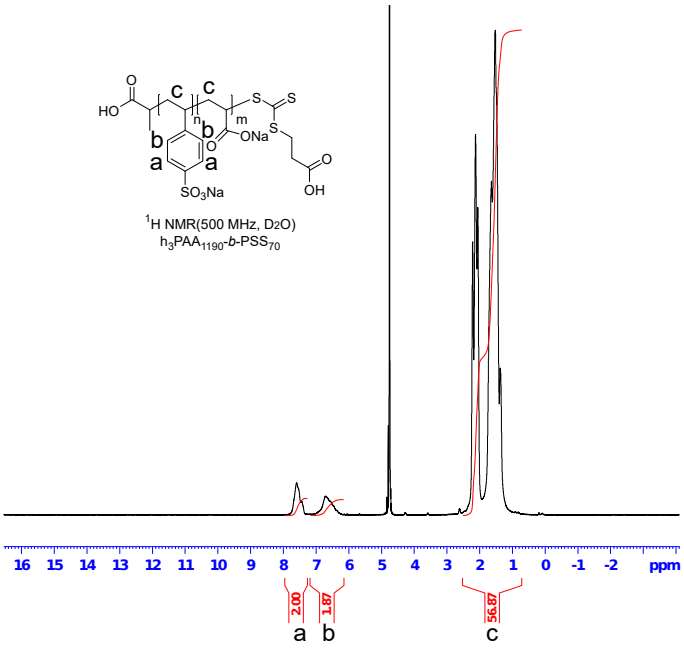

Figure S2: ^{1}H NMR spectrum of $h_3{-}PA_{1190}PSS_{70}$ in D_2O.

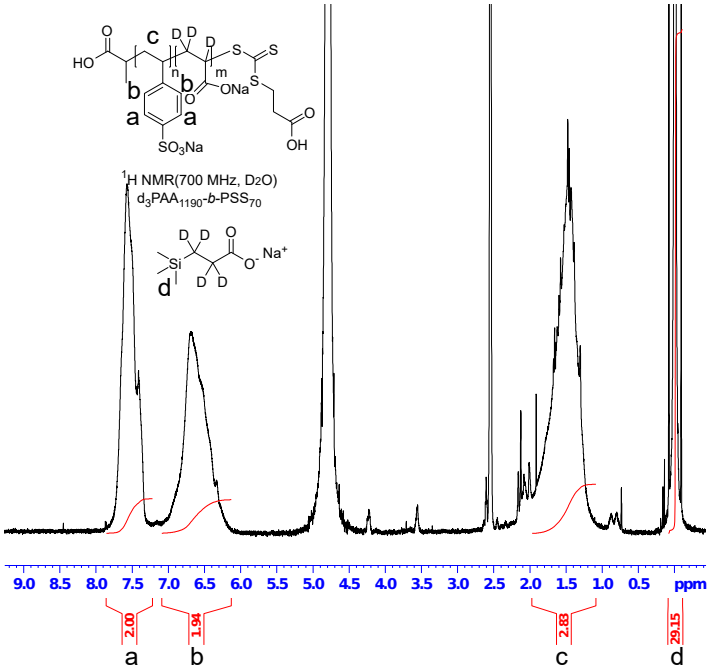

Figure S3: ^{1}H NMR spectrum of d_3−$PA_{1190}PSS_{70}$ in D_2O.

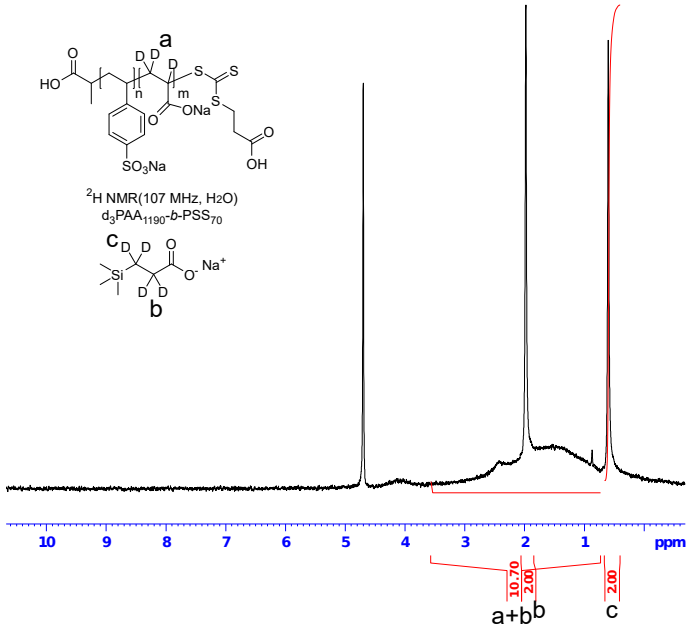

Figure S4: ^{2}H NMR spectrum of d_3−$PA_{1190}PSS_{70}$ in H_2O.

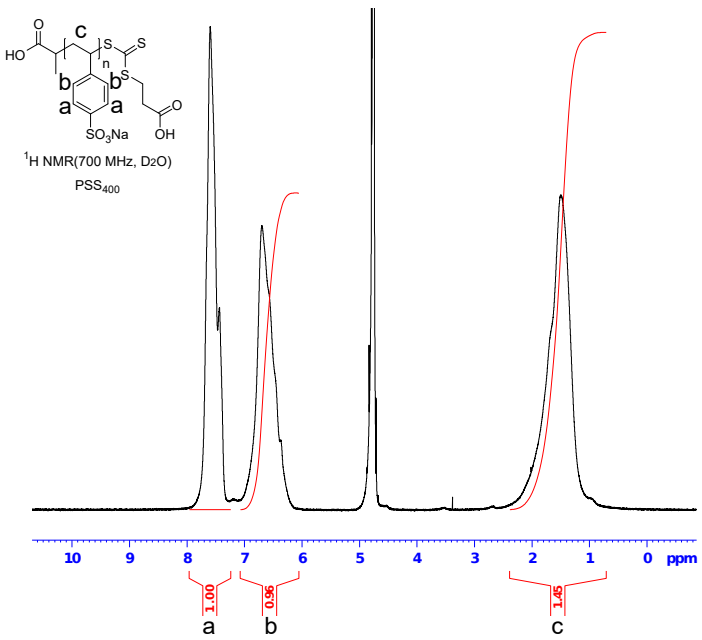

Figure S5: ^{1}H NMR spectrum of PSS_{400} in D_2O.

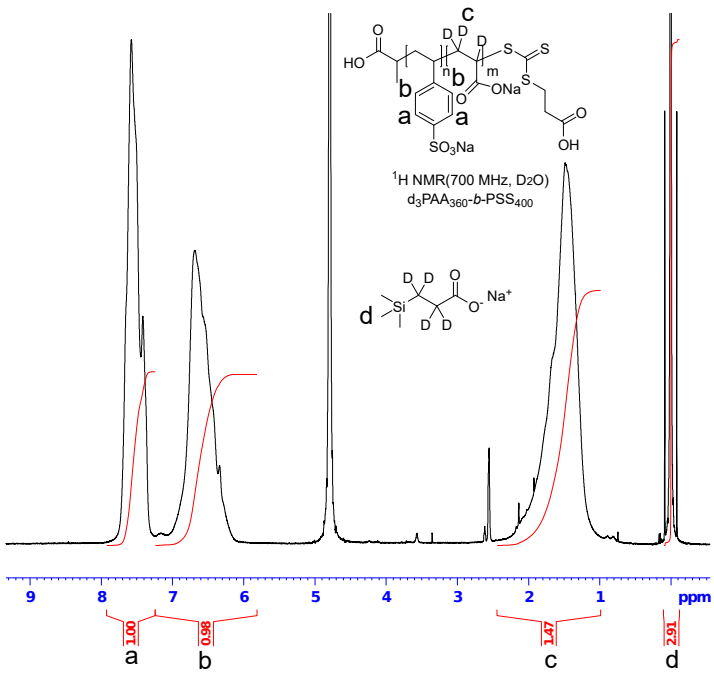

Figure S6: ^{1}H NMR spectrum of $d_3{-}PA_{360}PSS_{400}$ in D_2O.

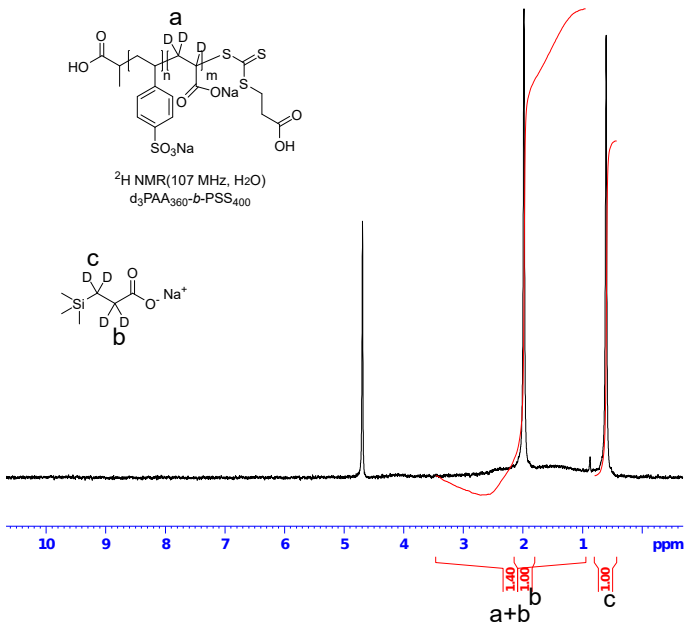

Figure S7: ^{2}H NMR spectrum of $d_3-PA_{360}PSS_{400}$ in H_2O.

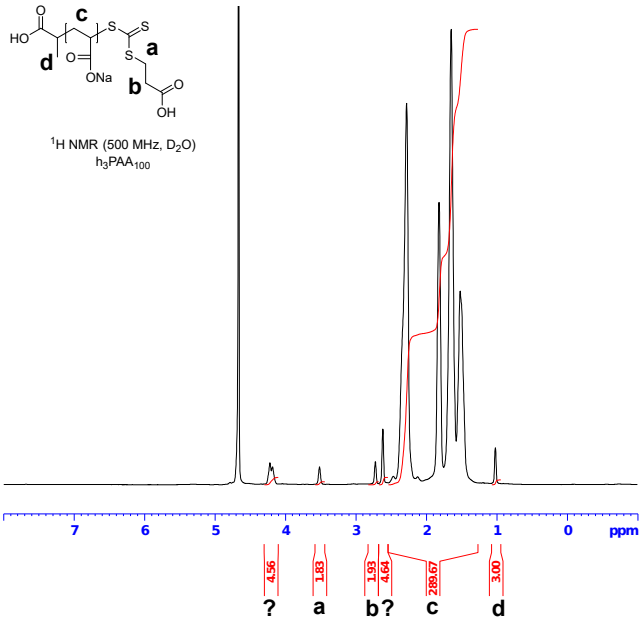

Figure S8: ^{1}H NMR spectrum of h_3-PA_{100} in D_2O.

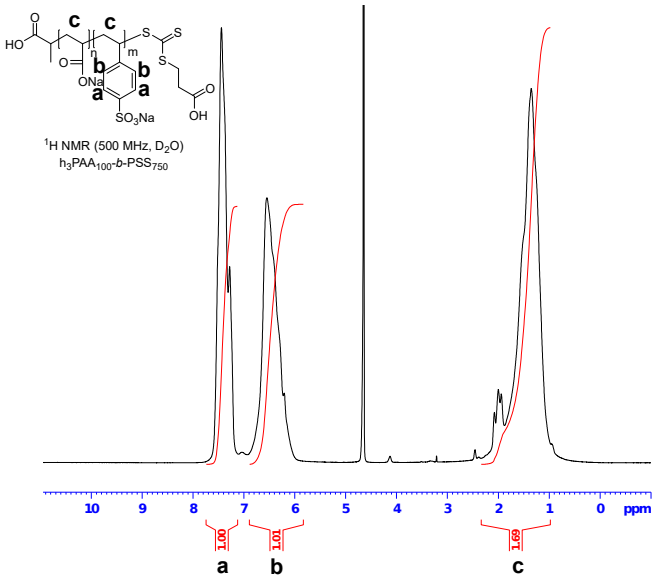

Figure S9: ^{1}H NMR spectrum of $h_3{-}PA_{100}PSS_{750}$ in D_2O.

2.2 Static and dynamic light scattering

The intensity-time correlation function $g_2(\tau) - 1$ measured with dynamic light scattering was analyzed using the method of cumulants[12]

$$g_2(\tau) - 1 = B + \beta \exp\left(-2\Gamma\tau\right)\left(1 + \frac{\mu_2}{2!}\tau^2\right)^2 \tag{S2}$$

B is a factor correcting the baseline, β a factor, which depends on the experimental setup, Γ the relaxation rate and μ_2 the the second cumulant. The apparent diffusion coefficient $D_{app}(c, q)$ for a given q is calculated according to

$$D_{app} = \frac{\Gamma}{q^2} \tag{S3}$$

The diffusion coefficient is consequently extrapolated towards $q = 0$ and $c = 0$ according to[13,14]

$$D_0 = D_{app}(c, q)\left(1 + CR_g^2q^2 + k_Dc\right) \tag{S4}$$

where C and k_D are constants describing q and the concentration dependence of D_0, respectively. The diffusion coefficient D_0 is used to calculate the hydrodynamic radius R_h using the Stokes-Einstein equation

$$R_h = \frac{k_B T}{6\pi\eta D_0} \tag{S5}$$

where T is the temperature, k_B the Boltzmann constant and η the viscosity of the solvent. Static light scattering was evaluated with the Zimm equation[15]

$$\frac{Kc}{\Delta R_\theta} = \frac{1}{M_w} + 2A_2 c + \frac{R_g^2}{3M_w} q^2 \tag{S6}$$

where c is the mass concentration of the polymer, M_w the weight average molecular weight of the polymer, A_2 the second osmotic virial coefficient and R_g the radius of gyration. ΔR_θ is the Rayleigh ratio and identical with the macroscopic scattering cross-section $\frac{d\Sigma}{d\Omega}$ used to express the scattering intensity in SANS and SAXS. K is the contrast factor given by

$$K = \frac{4\pi^2}{N_A \lambda_0^4} \left(n_{\text{standard}} \frac{dn}{dc} \right)^2 \tag{S7}$$

It contains the Avogadro constant N_A, the wavelength of the laser in vacuo λ_0, the refractive index of the standard (in this case toluene) n_{standard} and the refractive index increment of the polymer in the solvent $\frac{dn}{dc}$.

Figure S10–S12 show the characterization of the used polymers with static and dynamic light scattering. As solvent we choose an aqueous solution of 100 mmol L^{-1} NaCl at pH 9. In sub-figure A of each graph one can find the extrapolation of the diffusion coefficient to $c = 0$ and $q = 0$. The blue points indicate the extrapolation towards $q = 0$ for a given concentration. The blue line indicates the extrapolation of these points towards $c = 0$. The intercept defines D_0, which we used to calculate the hydrodynamic radius R_h. Similarly, figure B shows the extrapolation of the static light scattering data towards $c = 0$ and $q = 0$.

Figure C shows the measurement of the refractive index increment for this given polymer

in the same solvent conditions. The refractive index increment $\frac{dn}{dc}$ was determined using a differential refractometer (DR3 by SLS Systemtechnik, Denzlingen, Germany). The instrument operates at a wavelength of $\lambda_0 = 635\,\mathrm{nm}$. A stock solution of $10\,\mathrm{g\,L^{-1}}$ polymer was prepared in $100\,\mathrm{mmol\,L^{-1}}$ NaCl (H_2O), adjusted to pH 9 and dialyzed against the solvent solution prior to dilution.[16] The measured values of $\frac{dn}{dc}$ can be found in Table S1.

Table S1 summarizes the results from the light scattering characterization.

Table S1: Results from the light scattering analysis of the used polymers in aqueous 100 mmol L^{-1} NaCl solution in the absence of $CaCl_2$.

Polymer	c /g L^{-1}	D_0/nm^2 s^{-1}	R_h/nm	R_g/nm	M_w/kg mol^{-1}	$A_2/10^4$cm^3 mol g^{-2}	k_D/cm^3 g^{-1}	R_g/R_h	dn/dc/cm^3 g^{-1}
h_3−$PA_{1190}PSS_{70}$	1.50	25370 ± 363	9.8 ± 0.1	13.4 ± 0.6	62835 ± 139				
	1.25	23802 ± 311	10.4 ± 0.1	15.2 ± 0.6	68633 ± 153				
	1.00	23013 ± 349	10.8 ± 0.2	14.7 ± 0.7	78395 ± 241				
	0.75	21495 ± 377	11.5 ± 0.2	17.5 ± 0.7	90381 ± 346				
	0.00	17871 ± 765	13.9 ± 0.6	23.5 ± 1.9	160093 ± 2117	32.6 ± 0.3	275 ± 48	1.7 ± 0.2	0.172 ± 0.001
d_3−$PA_{1190}PSS_{70}$	1.50	25723 ± 316	9.6 ± 0.1	14.3 ± 0.8	69549 ± 254				
	1.25	25359 ± 409	9.8 ± 0.2	14.8 ± 0.6	77736 ± 187				
	1.00	23515 ± 215	10.5 ± 0.1	14.6 ± 0.6	87389 ± 232				
	0.75	21883 ± 328	11.3 ± 0.2	18.9 ± 0.9	100969 ± 510				
	0.00	18249 ± 637	13.6 ± 0.5	24.0 ± 2.4	181393 ± 3170	29.5 ± 0.4	284 ± 41	1.8 ± 0.2	0.157 ± 0.001
d_3−$PA_{360}PSS_{400}$	1.50	27812 ± 185	8.9 ± 0.1	21.0 ± 0.6	87076 ± 326				
	1.25	27186 ± 187	9.1 ± 0.1	18.3 ± 0.6	89987 ± 264				
	1.00	26698 ± 290	9.3 ± 0.1	18.7 ± 0.7	96787 ± 363				
	0.75	25814 ± 248	9.6 ± 0.1	18.2 ± 0.7	102784 ± 353				
	0.00	23951 ± 486	10.4 ± 0.2	13.8 ± 2.4	126661 ± 1208	12.4 ± 0.3	108 ± 19	1.3 ± 0.2	0.177 ± 0.001
h_3−$PA_{100}PSS_{750}$	1.50	23733 ± 114	10.5 ± 0.1	16.3 ± 0.4	127905 ± 274				
	1.25	23155 ± 229	10.7 ± 0.1	17.5 ± 0.5	138356 ± 383				
	1.00	22334 ± 179	11.1 ± 0.1	17.7 ± 0.4	149516 ± 314				
	0.75	20641 ± 84	11.7 ± 0.1	18.5 ± 0.4	161840 ± 434				
	0.00	17669 ± 198	14.0 ± 0.2	21.6 ± 2.3	220195 ± 1628	10.7 ± 0.1	231 ± 13	1.5 ± 0.2	0.174 ± 0.001

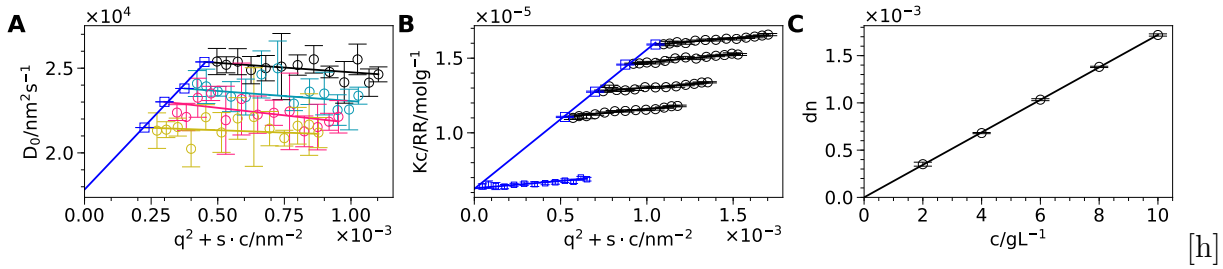

[h]

Figure S10: (**A**) Dynamic Zimm plot of $h_3-PA_{1190}PSS_{70}$ in 100 mmol L^{-1} NaCl. (**B**) Zimm plot of $h_3-PA_{1190}PSS_{70}$ in 100 mmol L^{-1} NaCl. (**C**) Refractive index increment as a function of concentration of $h_3-PA_{1190}PSS_{70}$ in 100 mmol L^{-1} NaCl.

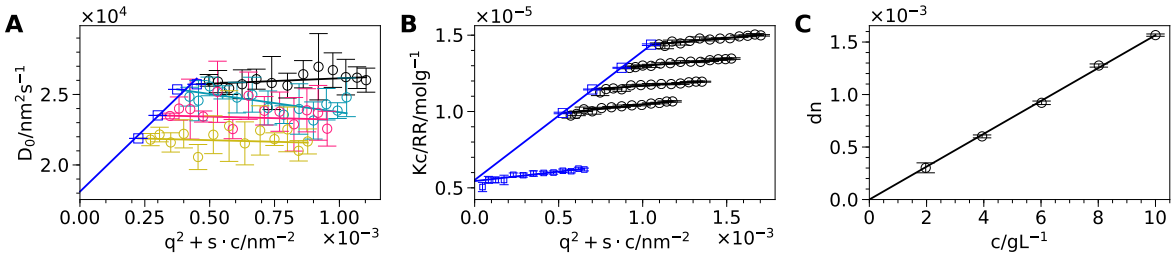

Figure S11: (**A**) Dynamic Zimm plot of $d_3-PA_{1190}PSS_{70}$ in 100 mmol L^{-1} NaCl. (**B**) Zimm plot of $d_3-PA_{1190}PSS_{70}$ in 100 mmol L^{-1} NaCl. (**C**) Refractive index increment as a function of concentration of $d_3-PA_{1190}PSS_{70}$ in 100 mmol L^{-1} NaCl.

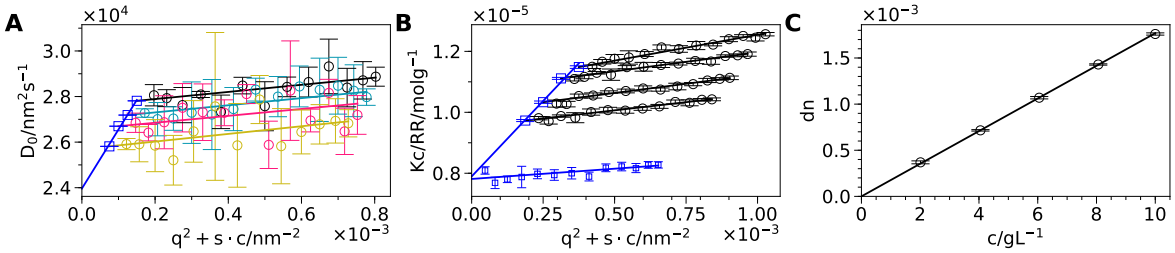

Figure S12: (**A**) Dynamic Zimm plot of $d_3-PA_{360}PSS_{400}$ in 100 mmol L^{-1} NaCl. (**B**) Zimm plot of $d_3-PA_{360}PSS_{400}$ in 100 mmol L^{-1} NaCl. (**C**) Refractive index increment as a function of concentration of $d_3-PA_{360}PSS_{400}$ in 100 mmol L^{-1} NaCl.

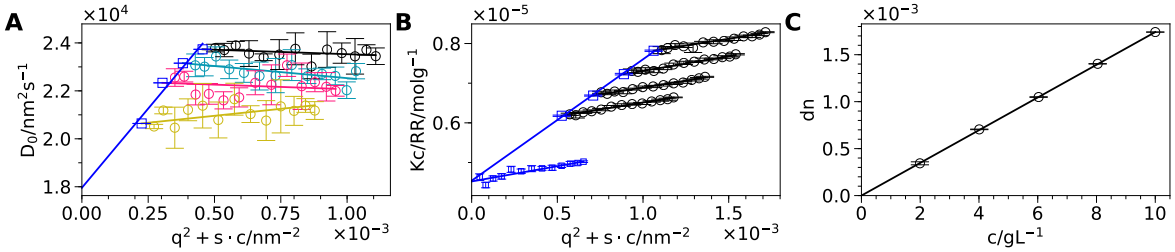

Figure S13: (**A**) Dynamic Zimm plot of $h_3-PA_{100}PSS_{750}$ in 100 mmol L^{-1} NaCl. (**B**) Zimm plot of $h_3-PA_{100}PSS_{750}$ in 100 mmol L^{-1} NaCl. (**C**) Refractive index increment as a function of concentration of $h_{100}-PA_{360}PSS_{750}$ in 100 mmol L^{-1} NaCl.

3 Reversibility of micelle formation

The reversibility of micelle formation was shown by addition of Na_2EDTA to a micelle solution. For this an aqueous 200 mmol L^{-1} solution of Na_2EDTA was prepared and adjusted to pH 9 using 1 mol L^{-1} NaOH. In addition, an aqueous 200 mmol L^{-1} $CaCl_2$ solution was prepared and adjusted to pH 9 using 100 mmol L^{-1} NaOH solution. Both solutions were filtered using hydrophilic 100 nm PVDF filters (Merck Millipore).

First, a solution of $h_3-PA_{1190}PSS_{70}$ (1 g L^{-1}, pH 9, 1 mL) in 100 mmol L^{-1} NaCl was investigated using angular dependent DLS and SLS. To this solution an aliquot of 50 µL $CaCl_2$ solution was added to trigger micelle formation. Subsequently, aliquots of 25 µL of Na_2EDTA or $CaCl_2$ solution were added to switch between single chains and micelles. After each injection angular dependent DLS and SLS was performed. Four complete cycles were carried out. This increased the total volume of 1000 µL to 1225 µL.

Figure S14 shows the hydrodynamic radius R_h from DLS upon subsequent additions of

Ca^{2+} and EDTA.

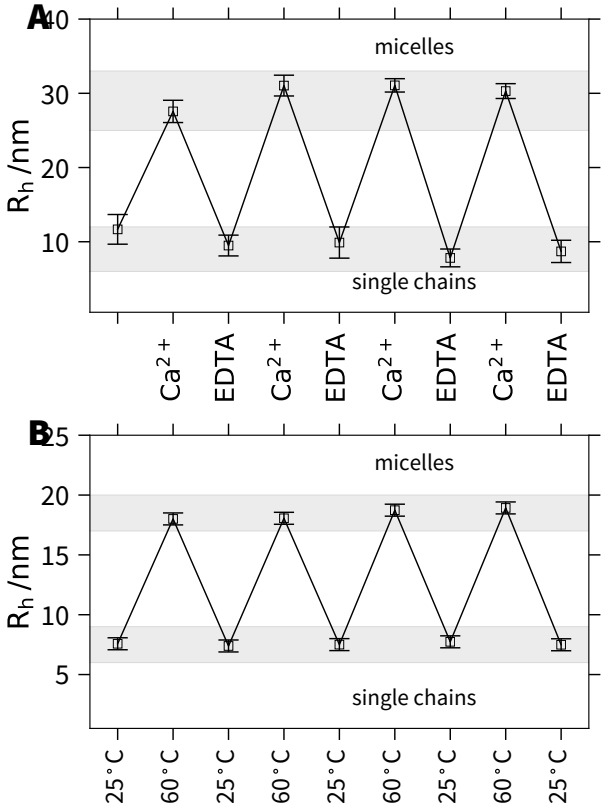

Figure S14: (**A**) Hydrodynamic radius R_h as a function of subsequent injections of $CaCl_2$ and Na_2EDTA. The first point refers to a solution of $1\,g\,L^{-1}$ $h_3{-}PA_{1190}PSS_{70}$ in $100\,mmol\,L^{-1}$ NaCl. (**B**) Hydrodynamic radius R_h as a function of temperature cycles between 25 °C and 65 °C for $h_3{-}PA_{1190}PSS_{70}$ at a polymer concentration of $1\,g\,L^{-1}$ and a Ca^{2+} concentration of $6.1\,mmol\,L^{-1}$.

We also showed the reversibility of micelle formation by a change in temperature. For this we prepared a sample of $h_3{-}PA_{1190}PSS_{70}$ at $1\,g\,L^{-1}$ and a concentration of Ca^{2+} of $6.1\,mmol\,L^{-1}$. This sample is close to the micelle transition but still in the single chain regime. Upon an increase of temperature the binding of Ca^{2+} to the PA block is promoted and micellization occurs. Various temperature cycles combined with angular dependent SLS and DLS were performed. Figure S14B shows the hydrodynamic radius for those experiments.

4 Scattering length densities

Table S2 shows the molar volumes V_m, scattering length b and scattering length densities ρ for neutrons and X-rays (at 12.46 keV) used for the analysis of the data. The scattering length density of a given compound is given by

$$\rho = \frac{b}{V_m} N_a \tag{S8}$$

with N_A being the Avogadro constant.

Table S2: Molar volumes, neutron and X-ray scattering length and scattering length density of the used compounds. $\rho_{\text{X-rays}}$ was calculated for a X-ray energy of 12.46 keV.

Compound	V_m /cm^3 mol^{-1}	b_{neutrons} /fm	$b_{\text{X-Rays}}$ /fm	ρ_{neutrons} /$1 \cdot 10^{-10}$ cm^{-2}/	$\rho_{\text{X-rays}}$ /$1 \cdot 10^{-14}$ cm^{-2}
h_3PA^-	29.1[a]	20.327	107.269	4.208	22.21
d_3PA^-	29.1[a]	51.557	107.269	10.674	22.21
NaPSS	108.7	50.881	299.823	2.818	16.61
D_2O	18.141	19.145	28.242	6.355	9.375
H_2O	18.069	−1.675	28.242	−0.558	9.398
Ca^{2+}	17.0 ± 2.8[b]	4.7	51.652	1.665	$1.830 \cdot 10^{-3}$
$d_3{-}PA_{1190}PSS_{70}$[c]			7.762		
$d_3{-}PA_{360}PSS_{400}$[c]			4.165		

[a] Taken from reference 17. [b] The molar volume of Ca^{2+} was fitted. The shown value is the average value we obtained from analysis of the three different polymers. [c] We assumed that every PA monomer is complexed by 0.5 equivalents of Ca^{2+}.

5 Analysis of scattering data

5.1 Form factor model

The form factor of self-assembled block copolymers with excluded volume interaction of the polymer chains was first treated by Pedersen under the assumption that the polymers form spherical micellar-like structures.[18–21] The macroscopic scattering cross-section $\frac{d\Sigma}{d\Omega}(q)$ of a

solution of micelles can be written as[20]

$$\frac{d\Sigma}{d\Omega}(q) = N\left[N_{\mathrm{agg}}^2\beta_{\mathrm{core}}^2 A_{\mathrm{core}}^2(q) + N_{\mathrm{agg}}\beta_{\mathrm{corona}}^2 P'_{\mathrm{corona}}(q) + 2N_{\mathrm{agg}}^2\beta_{\mathrm{core}}\beta_{\mathrm{corona}}A_{\mathrm{core}}(q)\,A_{\mathrm{corona}}(q) + N_{\mathrm{agg}}\left(N_{\mathrm{agg}} - P'_{\mathrm{corona}}(0)\right)\beta_{\mathrm{corona}}^2 A_{\mathrm{corona}}^2(q)\right] \tag{S9}$$

where N is the number density of micelles, N_{agg} the aggregation number of micelles, β_{core} and β_{corona} are the total excess scattering length of the block forming the spherical core and the corona, respectively. They are defined as

$$\beta_{\mathrm{corona}} = V_{\mathrm{m,\ corona}}\mathrm{DP}_{\mathrm{corona}}\Delta\rho_{\mathrm{corona}} \tag{S10}$$

and

$$\beta_{\mathrm{core}} = V_{\mathrm{m,\ core}}\mathrm{DP}_{\mathrm{core}}\Delta\rho_{\mathrm{core}} \tag{S11}$$

with V_{m} being the molecular volume of the respective monomer unit, $\mathrm{DP}_{\mathrm{corona}}$ and $\mathrm{DP}_{\mathrm{core}}$ the degree of polymerization of the corona and core block and $\Delta\rho$ the corresponding excess scattering length density.

Equation S9 consists of four different contributions: scattering from the spherical homogeneous core $A_{\mathrm{core}}^2(q)$, scattering from the polymer chains in the corona $P'_{\mathrm{corona}}(q)$, the cross-term between core and corona $A_{\mathrm{core}}(q)\cdot A_{\mathrm{corona}}(q)$ and the cross-term between different chains $A_{\mathrm{corona}}^2(q)$. $A_{\mathrm{core}}(q)$ is the scattering amplitude of a homogeneous sphere[22] with radius R_{core}

$$A_{\mathrm{core}}(q) = 3\frac{\sin(qR_{\mathrm{core}}) - qR_{\mathrm{core}}\cos(qR_{\mathrm{core}})}{(qR_{\mathrm{core}})^3} \tag{S12}$$

$P'_{\mathrm{corona}}(q)$ is the form factor of a chain in the corona. It contains the self-correlation of the chain $P_{\mathrm{exv}}(q)$ as well as the interaction between the chains, which is expressed by the interaction parameter ν[20,23]

$$P'_{\mathrm{corona}}(q) = \frac{P_{\mathrm{exv}}(q)}{1 + \nu P_{\mathrm{exv}}(q)} \tag{S13}$$

where $P_{\mathrm{exv}}(q)$ is the form factor of a semi flexible self-avoiding chain. This form factor

was first derived by Pedersen and Schurtenberger[24] and later corrected.[25] In experiments ν typically adopts values between 0 and 8 and is related to the osmotic compressibility κ by[20,23,26]

$$\kappa = 1 + \nu \tag{S14}$$

$A_{\text{corona}}(q)$ is given by

$$A_{\text{corona}}(q) = \frac{\int \rho_{\text{corona}}(r) r^2 \frac{\sin(qr)}{qr} dr}{\int \rho_{\text{corona}}(r) r^2 dr} \tag{S15}$$

with $\rho_{\text{corona}}(r)$ as the scattering length density profile in the corona. In this work we use a Gaussian profile, which is defined as

$$\rho_{\text{corona}}(r) = \begin{cases} 0 & \text{for } r < R_{\text{core}} \\ 1 & \text{for } r = R_{\text{core}} \\ \exp\left(\frac{-(r-R_{\text{core}})^2}{2s^2}\right) & \text{for } r > R_{\text{core}} \end{cases} \tag{S16}$$

with s controlling the thickness of the corona.

In order to take into account the size distribution of micelles we assumed a log-normal distribution of the aggregation number N_{agg}

$$p(N_{\text{agg}}) = \frac{1}{H\sqrt{2\pi}N_{\text{agg}}} \exp\left(\frac{-\log(N_{\text{agg}} - M)^2}{2H^2}\right) \tag{S17}$$

where H and M define the distribution and are connected to the mean aggregation number $\overline{N_{\text{agg}}}$ and standard deviation $\sigma_{\overline{N_{\text{agg}}}}$ by

$$\overline{N_{\text{agg}}} = \exp\left(M + \frac{H^2}{2}\right) \tag{S18}$$

$$\sigma_{\overline{N_{\text{agg}}}} = \sqrt{\exp(H^2 + 2M)(\exp(H^2) - 1)} \tag{S19}$$

The macroscopic scattering cross-section is therefore

$$\frac{d\Sigma}{d\Omega}_{\text{polydisperse}}(q) = \int \frac{d\Sigma}{d\Omega}(q)p(N_{\text{agg}})dN_{\text{agg}} \tag{S20}$$

Instrumental resolution for SANS has been taken into account according to Ref. 27. The macroscopic scattering function is convoluted with a resolution function $R(q, \sigma_q)$, which depends on wavelength spread, finite collimation of the beam and detector resolution

$$\frac{d\Sigma}{d\Omega}_{\text{smeared}}(q) = \int R(q, \sigma_q)\frac{d\Sigma}{d\Omega}_{\text{polydisperse}}(q)dq \tag{S21}$$

5.2 Fitting procedure

For the form factor fits we used the SASET program,[28] which allows global fitting of several contrasts at the same time. During the data analysis of the SANS curves we took into account the instrumental resolution for each detector configuration and merged the data only for final representation. This approach allows us to increase the number of available data points since we do not truncate the data in the region of overlapping q. We performed a global fit to the SANS and SAXS data with a single set of shared fitting parameters. For the samples, where the aggregation number changes with D_2O content we attributed a common aggregation number to the corresponding SANS and SAXS curves but left the rest of the fitting parameters as global fitting parameters.

In order to constrain the fit we used the molar volumes of the individual blocks, known from the degree of polymerization and the molar volumes listed in Table S2. Moreover, we restricted the fit by giving the used polymer concentration. Together with the aggregation number N_{agg} (which is a fitting parameter) the number density N of micelles in L^{-1} is directly obtained by

$$N = \frac{c}{M_{\text{polymer}}N_{\text{agg}}}N_A \tag{S22}$$

with c the polymer concentration in $g\,L^{-1}$, the molecular weight of the polymer M_{polymer} and

the aggregation number N_{agg}.

5.3 SAXS

Figure S15 and S16 show the SAXS profiles of $d_3-PA_{1190}PSS_{70}$ and $d_3-PA_{360}PSS_{400}$ micelles in the presence of Ca^{2+} at various D_2O/H_2O ratios. The solid lines represents a fit to the previously described form factor model. For the sample $d_3-PA_{1190}PSS_{70}$ we obtained a change in aggregation number when changing from H_2O to D_2O. Figure S15 shows the aggregation numbers obtained from the form factor analysis as a function of D_2O content.

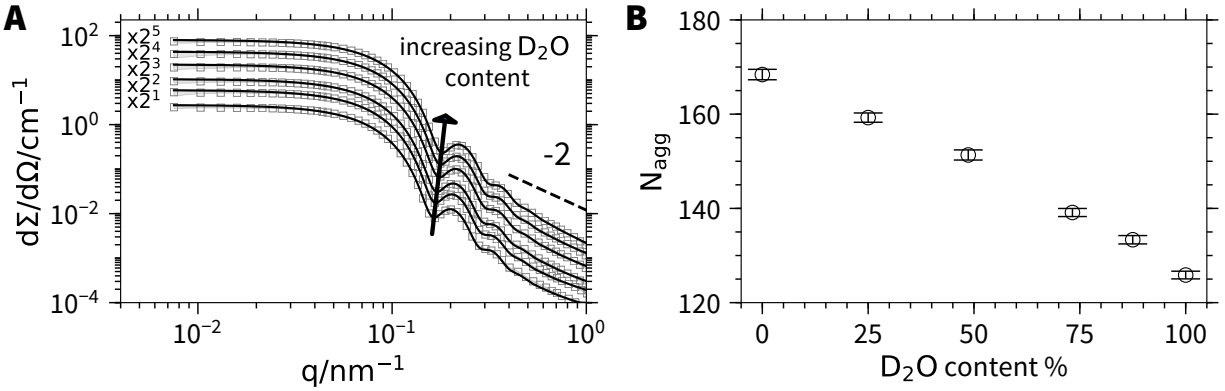

Figure S15: SAXS profiles of $d_3-PA_{1190}PSS_{70}$ micelles ($c_{poly} = 4\,g\,L^{-1}$, $c_{Ca^{2+}} = 25\,mmol\,L^{-1}$) at various D_2O/H_2O ratios. The solid lines represent fits to the form factor of a polydisperse block copolymer micelle.[20] An overview of the fit results can be found in Table S3.

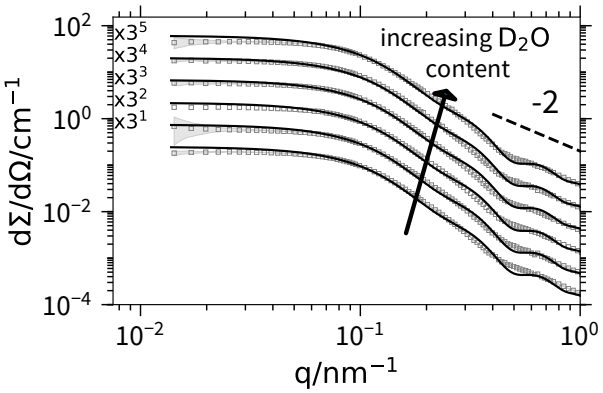

Figure S16: SAXS profiles of $d_3-PA_{360}PSS_{400}$ ($c_{poly} = 4\,g\,L^{-1}$, $c_{Ca^{2+}} = 50\,mmol\,L^{-1}$) at various D_2O/H_2O ratios. The solid lines represent fits to the form factor of a polydisperse block copolymer micelle.[20] An overview of the fit results can be found in Table S3.

Table S3: Parameters for the micelles in the presence of $CaCl_2$ obtained for the fits shown in the main manuscript and in Figure S15 and S16.

D_2O %		N_{agg}	$\sigma_{N_{agg}}/N_{agg}$	R_{core}/nm	$\sigma_{R_{core}}/R_{core}$	$R_{g,corona}$/nm	s/nm	ν	h	$V_{m,\ Ca^{2+}}$/cm^3 mol^{-1}	$\frac{d\Sigma}{d\Omega}_{inc}$/cm^{-1}
d_3−PA_{1190}-PSS_{70}											
0.0	SANS	168.40 ± 0.11	$0.31 \pm 1.5 \cdot 10^{-4}$	26.10 ± 0.02	$0.102 \pm 5.0 \cdot 10^{-5}$	2.12 ± 0.03	$4.05 \pm 8.9 \cdot 10^{-3}$	$0.00 \pm 7.4 \cdot 10^{-3}$	11.59 ± 0.01	13.9 ± 0.02	$2.7 \cdot 10^{-3} \pm 1.4 \cdot 10^{-4}$
0.0	SAXS										—
25.0	SANS	159.27 ± 0.10		25.63 ± 0.02							$1.3 \cdot 10^{-3} \pm 1.1 \cdot 10^{-4}$
25.0	SAXS										—
48.6	SANS	151.34 ± 0.11		25.20 ± 0.02							$2.1 \cdot 10^{-3} \pm 7.5 \cdot 10^{-5}$
48.6	SAXS										—
73.3	SANS	139.13 ± 0.09		24.51 ± 0.02							$1.5 \cdot 10^{-3} \pm 4.9 \cdot 10^{-5}$
73.3	SAXS										—
87.5	SANS	133.35 ± 0.09		24.17 ± 0.02							$1.7 \cdot 10^{-3} \pm 3.3 \cdot 10^{-5}$
87.5	SAXS										—
100.0	SANS	125.86 ± 0.08		23.71 ± 0.02							$2.8 \cdot 10^{-13} \pm 2.3 \cdot 10^{-5}$
100.0	SAXS										—
d_3−PA_{360}-PSS_{400}											
0.0	SANS	19.6 ± 0.07	$0.21 \pm 9.9 \cdot 10^{-3}$	8.78 ± 0.03	$0.069 \pm 3.3 \cdot 10^{-3}$	9.55 ± 0.04	$8.86 \pm 9.5 \cdot 10^{-3}$	$1.19 \pm 2.3 \cdot 10^{-2}$	12.21 ± 0.03	19.6 ± 0.05	$2.0 \cdot 10^{-2} \pm 1.8 \cdot 10^{-4}$
0.0	SAXS										—
25.0	SANS										$4.4 \cdot 10^{-3} \pm 1.3 \cdot 10^{-4}$
25.0	SAXS										—
48.6	SANS										$4.4 \cdot 10^{-3} \pm 9.2 \cdot 10^{-5}$
48.6	SAXS										—
65.8	SANS										$3.0 \cdot 10^{-3} \pm 6.8 \cdot 10^{-5}$
65.8	SAXS										—
80.0	SANS										$1.5 \cdot 10^{-3} \pm 4.5 \cdot 10^{-5}$
80.0	SAXS										—
100.0	SANS										$8.6 \cdot 10^{-4} \pm 5.7 \cdot 10^{-5}$
100.0	SAXS										—

5.4 Model with PSS in the core and d_3−PA in the corona

Figure S18 shows the SANS profiles of d_3−$PA_{360}PSS_{400}$ and the model fit with PSS in the core and d_3−PA in the corona. This model can not describe the scattering data sufficiently well.

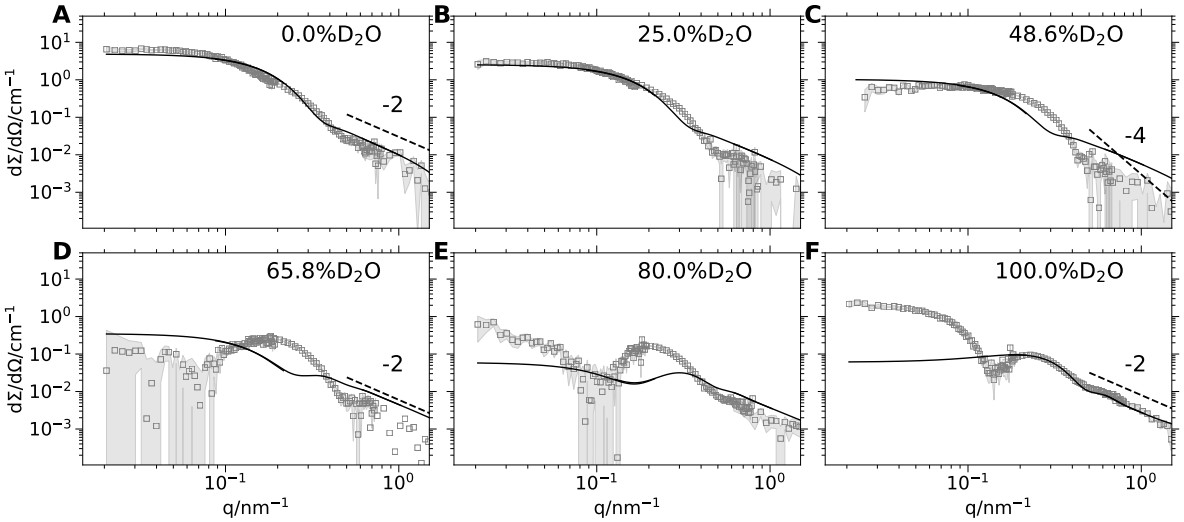

Figure S17: SANS profiles of d_3−$PA_{360}PSS_{400}$ micelles at various D_2O/H_2O ratios. The solid lines represents fits to the form factor of a polydisperse block copolymer with PSS in the core and d_3−PA in the corona.

6 Phase diagrams of the polymers in the presence of Ca^{2+}

The phase diagrams were established by subsequent addition of aliquots of 20 µL of a 50 mmol L^{-1} $CaCl_2$ solution to 1 mL of a solution of block copolymer in 100 mmol L^{-1} NaCl. The transition from single chains to micelles was monitored by turbidity using a UV-Vis spectrometer at 400 nm or the static light scattering signal (using the ALV-CSG3 at a scattering angle of 150°). Figure S18A shows the phase diagram with the points indicating single chain, micelle and phase separation regime. The phase boundaries for d_3−$PA_{1190}PSS_{70}$ and h_3−$PA_{1190}PSS_{70}$ were found to be identical within the given accuracy of the $CaCl_2$

injections. For $d_3-PA_{1190}PSS_{70}/h_3-PA_{1190}PSS_{70}$ precipitation of the micelles from solution can be found at $CaCl_2$ concentrations above 50 mmol L^{-1}, which we attribute to strong screening of the PSS chains in the corona and consequent destabilization of the micelles. $h_3-PA_{100}PSS_{750}$ does not form micelles in the presence of Ca^{2+}. Figure S18B shows a SAXS profile (D2AM, ESRF Grenoble) of $h_3-PA_{100}PSS_{750}$ in 50 mmol L^{-1} $CaCl_2$ solution. The scattering can be well described by the model of a generalized Gaussian chain[29]. We obtain a radius of gyration R_g of 14.0 ± 0.1 nm and a Flory exponent ν of 0.57 ± 0.05, which indicates that the polymer chains do not aggregate.

Figure S18C shows an autocorrelation function of $h_3-PA_{1190}PSS_{70}$ micelles and the corresponding fit using eq S2. The correlation function shows a mono modal decay, from which we conclude that the majority of polymers are aggregates into micelles and the fraction of free polymer is negligible.

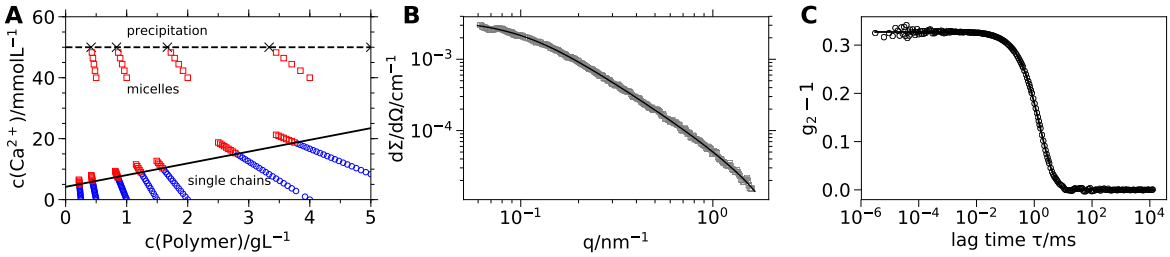

Figure S18: **A** Phase diagram of $d_3-PA_{1190}PSS_{70}/h_3-PA_{1190}PSS_{70}$ in the presence of Ca^{2+} in H_2O. The symbols indicate the compositions, which were prepared to identify the phase diagram. Black crosses indicate precipitates, red squares micelles and blue circles single chains. **B** SAXS profile (D2AM, ESRF Grenoble) of $h_3-PA_{100}PSS_{750}$ at 1 g L^{-1} in 50 mmol L^{-1} $CaCl_2$. The solid line represents the fit to the generalized Gaussian chain model[29]. **C** Exemplary autocorrelation function of $h_3-PA_{1190}PSS_{70}$ micelles and fit to eq S2.

References

(1) Yap, H. P.; Hao, X.; Tjipto, E.; Gudipati, C.; Quinn, J. F.; Davis, T. P.; Barner-Kowollik, C.; Stenzel, M. H.; Caruso, F. Synthesis, multilayer film assembly, and capsule formation of macromolecularly engineered acrylic acid and styrene sulfonate block copolymers. *Langmuir* **2008**, *24*, 8981–8990, DOI: 10.1021/la8011074.

(2) Chaduc, I.; Crepet, A.; Boyron, O.; Charleux, B.; D'Agosto, F.; Lansalot, M. Effect of the pH on the RAFT Polymerization of Acrylic Acid in Water. Application to the Synthesis of Poly(acrylic acid)-Stabilized Polystyrene Particles by RAFT Emulsion Polymerization. *Macromolecules* **2013**, *46*, 6013–6023, DOI: 10.1021/ma401070k.

(3) Dao, V. H.; Cameron, N. R.; Saito, K. Synthesis of ultra-high molecular weight ABA triblock copolymers: Via aqueous RAFT-mediated gel polymerisation, end group modification and chain coupling. *Polym. Chem.* **2017**, *8*, 6834–6843, DOI: 10.1039/c7py01410d.

(4) Schweins, R.; Huber, K. Collapse of sodium polyacrylate chains in calcium salt solutions. *Eur. Phys. J. E* **2001**, *5*, 117–126, DOI: 10.1007/s101890170093.

(5) Lages, S.; Schweins, R.; Huber, K. Temperature-Induced Collapse of Alkaline Earth CationPolyacrylate Anion Complexes. *J. Phys. Chem. B* **2007**, *111*, 10431–10437, DOI: 10.1021/jp068258k.

(6) Schweins, R.; Lindner, P.; Huber, K. Calcium Induced Shrinking of NaPA Chains: A SANS Investigation of Single Chain Behavior. *Macromolecules* **2003**, *36*, 9564–9573, DOI: 10.1021/ma0347722.

(7) Goerigk, G.; Schweins, R.; Huber, K.; Ballauff, M. The distribution of Sr 2+ counterions around polyacrylate chains analyzed by anomalous small-angle X-ray scattering. *Europhys. Lett.* **2004**, *66*, 331–337, DOI: 10.1209/epl/i2003-10215-y.

(8) Schweins, R.; Goerigk, G.; Huber, K. Shrinking of anionic polyacrylate coils induced by Ca2+, Sr2+ and Ba2+: A combined light scattering and ASAXS study. *Eur. Phys. J. E* **2006**, *21*, 99–110, DOI: 10.1140/epje/i2006-10047-7.

(9) Orthaber, D.; Bergmann, A.; Glatter, O. SAXS experiments on absolute scale with Kratky systems using water as a secondary standard. *J. Appl. Crystallogr.* **2000**, *33*, 218–225, DOI: 10.1107/S0021889899015216.

(10) Boesecke, P. Reduction of two-dimensional small- and wide-angle X-ray scattering data. *J. Appl. Crystallogr.* **2007**, *40*, 423–427, DOI: 10.1107/S0021889807001100.

(11) Zemb, T.; Lindner, P. *Neutrons, X-rays and light: scattering methods applied to soft condensed matter*; North-Holland, 2002.

(12) Frisken, B. J. Revisiting the method of cumulants for the analysis of dynamic light-scattering data. *Appl. Opt.* **2001**, *40*, 4087, DOI: 10.1364/AO.40.004087.

(13) Burchard, W.; Schmidt, M.; Stockmayer, W. H. Influence of Hydrodynamic Preaveraging on Quasi-Elastic Scattering from Flexible Linear and Star-Branched Macromolecules. *Macromolecules* **1980**, *13*, 580–587, DOI: 10.1021/ma60075a020.

(14) Burchard, W.; Schmidt, M.; Stockmayer, W. H. Information on Polydispersity and Branching from Combined Quasi-Elastic and Intergrated Scattering. *Macromolecules* **1980**, *13*, 1265–1272, DOI: 10.1021/ma60077a045.

(15) Zimm, B. H. The Scattering of Light and the Radial Distribution Function of High Polymer Solutions. *J. Chem. Phys.* **1948**, *16*, 1093–1099, DOI: 10.1063/1.1746738.

(16) Brüssau, R and Goetz, N and Mächtle, W and Stölting, J. Characterization of polyacrylate samples. *Tenside, surfactants, Deterg.* **1991**, *28*, 396–406.

(17) Tondre, C.; Zana, R. Apparent molal volumes of polyelectrolytes in aqueous solutions. *J. Phys. Chem.* **1972**, *76*, 3451–3459, DOI: 10.1021/j100667a026.

(18) Pedersen, J. S.; Gerstenberg, M. C. Scattering Form Factor of Block Copolymer Micelles. *Macromolecules* **1996**, *29*, 1363–1365, DOI: 10.1021/ma9512115.

(19) Pedersen, J. S.; Svaneborg, C. Scattering from block copolymer micelles. *Curr. Opin. Colloid Interface Sci.* **2002**, *7*, 158–166, DOI: 10.1016/S1359-0294(02)00044-4.

(20) Svaneborg, C.; Pedersen, J. S. Form Factors of Block Copolymer Micelles with Excluded-Volume Interactions of the Corona Chains Determined by Monte Carlo Simulations. *Macromolecules* **2002**, *35*, 1028–1037, DOI: 10.1021/ma011046v.

(21) Pedersen, J. S.; Svaneborg, C.; Almdal, K.; Hamley, I. W.; Young, R. N. A Small-Angle Neutron and X-ray Contrast Variation Scattering Study of the Structure of Block Copolymer Micelles:? Corona Shape and Excluded Volume Interactions. *Macromolecules* **2003**, *36*, 416–433, DOI: 10.1021/ma0204913.

(22) Rayleigh, L. Form factor of a homogenous sphere. *Proc. Roy. Soc. London* **1911**, *A84*, 25–38.

(23) Svaneborg, C.; Pedersen, J. S. Block copolymer micelle coronas as quasi-two-dimensional dilute or semidilute polymer solutions. *Phys. Rev. E* **2001**, *64*, 010802, DOI: 10.1103/PhysRevE.64.010802.

(24) Skov, J.; Schurtenberger, P.; Pedersen, J. S. Scattering Functions of Semiflexible Polymers with and without Excluded Volume Effects Excluded Volume Effects. *Macromolecules* **1996**, *9297*, 7602–7612, DOI: 10.1021/ma9607630.

(25) Chen, W. R.; Butler, P. D.; Magid, L. J. Incorporating intermicellar interactions in the fitting of SANS data from cationic wormlike micelles. *Langmuir* **2006**, *22*, 6539–6548, DOI: 10.1021/la0530440.

(26) Sommer, C.; Pedersen, J. S.; Garamus, V. M. Structure and interactions of block copoly-

mer micelles of brij 700 studied by combining small-angle X-ray and neutron scattering. *Langmuir* **2005**, *21*, 2137–2149, DOI: 10.1021/la047489k.

(27) Pedersen, J. S.; Posselt, D.; Mortensen, K. Analytical treatment of the resolution function for small-angle scattering. *J. Appl. Crystallogr.* **1990**, *23*, 321–333, DOI: 10.1107/S0021889890003946.

(28) Muthig, M.; Prévost, S.; Orglmeister, R.; Gradzielski, M. SASET: A program for series analysis of small-angle scattering data. *J. Appl. Crystallogr.* **2013**, *46*, 1187–1195, DOI: 10.1107/S0021889813016658.

(29) Hammouda, B. SANS from homogeneous polymer mixtures: A unified overview. *Polym. Charact.* **1993**, *106*, 87–133, DOI: 10.1007/BFb0025862.